ISSN 2176-5480

22nd International Congress of Mechanical Engineering (COBEM 2013)
November 3-7, 2013, Ribeirão Preto, SP, Brazil

EFFECTS OF OUTLET DUCT LENGTH AND SHAPE ON THE PERFORMANCE OF CYCLONE SEPARATORS

Ricardo de Vasconcelos Salvo
Technological Federal University of Parana - UTFPR. Av. Alberto Carazzai, 1640, Bloco GHI. Cornélio Procópio - Paraná - Brazil.
ricardosalvo@utfpr.edu.br

Francisco José de Souza
Federal University of Uberlandia - UFU. Av. João Naves de Ávila, 2121, Bloco 5P. Uberlândia - Minas Gerais - Brazil.
fjsouza@mecanica.ufu.br

Diego Alves de Moro Martins
Federal University of Uberlandia - UFU. Av. João Naves de Ávila, 2121, Bloco 5P. Uberlândia - Minas Gerais - Brazil.
moromartins@gmail.com

Abstract. *In most published studies regarding numerical simulation of cyclone separators, the outlet duct is usually treated as a short straight duct, differing considerably from the experimental apparatus, in which a relatively long duct followed by a curve, or vice-versa, is generally used. This work focus on the influence of length and shape of the outlet duct on the grade efficiency and pressure drop inside a small cyclone separator. The results are obtained through Large Eddy Simulation of the fluid flow inside the separator, coupled with a concomitant Lagrangian description of the dispersed phase. This methodology is free from ad-hoc constants, allowing a faithful representation of the gas-particle flow without the necessity of empirical parameters adjustment. Twenty seven different outlet duct configurations, including different lengths, curves, curves positions and curvature radii were simulated. The results show that the cyclone outlet duct is worth more attention than it has been given, as it substantially affects the cyclone performance*

Keywords: *Cyclone separator; Outlet duct; Large Eddy Simulation; Eulerian-Lagrangian.*

1. INTRODUCTION

Cyclones are widely used separator devices, being applied in many industrial branches, ranging from food and pharmaceutical industries to mining and petrochemical industries. Their popularity is based on their relative geometrical simplicity, low manufacturing, operational and maintenance costs. Despite their deceitful simplicity, cyclones are complicated to design and hardly optimized, since the flow field within them is extremely complex (Hoffmann and Stein, 2008). Due to this complexity, Computational Fluid Dynamics became, recently, an important tool in cyclone and hydrocyclone analysis and design by providing a detailed picture of the flow field inside these separators (Chuah *et al*., 2006; Azadi *et al*., 2010; Raoufi *et al*., 2008; Baskar *et al*., 2007; Schuetz *et al*., 2004; Shi and Bayless, 2007; Wan *et al*., 2008; Jiao *et al*., 2008; Hoekstra *et al*., 1999; Derksen 2003; Derksen *et al*., 2006; Derksen *et al*., 2008 - among others).

The effects of geometrical parameters on the flow and efficiency of cyclones have been studied with the aid of computational fluid dynamics by different researches over the past few years. Among these parameters we can highlight: the inlet duct entrance (Bernardo (2005); Bernardo *et al*., 2006; Zhao *et al*., 2006; Martignoni *et al*., 2007; Yoshida *et al*., 2005 and Yoshida *et al*., 2009); the outlet duct for the dispersed phase - including changes in the cone apex diameter (Chuah *et al*., 2006; Qian *et al*., 2006; Bhaskar *et al*., 2007; Dias *et al*., 2009; Yoshida *et al*., 2010; Elsayed and Lacor (2013)a); and changes in the diameter and length of the vortex finder (Noriler *et al*., 2004; Raoufi *et al*., 2008; Kepa (2010); Elsayed and Lacor (2013)b just to name a few). A specific parameter which has not received much attention is the overflow duct. To the best of the authors knowledge only Schmidt *et al*., 2004, were concerned to hold a work devoted, only, to the study of different configurations for the overflow duct.

Schmidt *et al*., 2004 found that modifications in the overflow duct may produce considerable changes in the flow field inside the cyclone separator. Unfortunately their work focused only on the gas phase, and no considerations regarding the dispersed phase were made. In the present work a large effort was made in an attempt to understand the impact of common overflow duct types - from an experimental and practical point of view - in the flow field and efficiency of a small cyclone separator. Thirty different configurations, including four different lengths, two curves - one 180 degrees curve and a 90 degrees curve - three different curves positions and curvature radii were numerically simulated. All the performed simulations were based on the LES (Large Eddy Simulation) methodology, with the dynamic turbulence model being applied to account for turbulence inside the cyclone. The simulations were concomitant, and the dispersed phase was computed in an Lagrangian reference frame while the gas phase was computed in an Eulerian framework. In general the obtained results show a complicated relation between the overflow duct length and shape and cyclone efficiency parameters, pressure drop and grade efficiency. The results show that even relatively simple changes in the cyclone outlet duct may considerably alter the cyclone efficiency.

ISSN 2176-5480

2. MATHEMATICAL MODELS

2.1 Gas phase model

The conservation of mass and the Navier-Stokes equations for a general incompressible, Newtonian flow can be written, adopting the Einstein convention, respectively as:

$$\frac{\partial \rho u_i}{\partial x_i} = 0 \tag{1}$$

$$\frac{\partial \rho u_i}{\partial t} + \frac{\partial}{\partial x_j}(\rho u_i u_j) = -\frac{\partial p}{\partial x_i} + \frac{\partial}{\partial x_j}\left[\mu\left(\frac{\partial u_i}{\partial x_j} + \frac{\partial u_j}{\partial x_i}\right)\right] \tag{2}$$

By applying a filtering process to the above equations, it is possible to separate the larger scales of motion, which are related to the lowest frequencies, from the smallest scales, which are related to the higher frequencies. Eq. (2) may then be rewritten as:

$$\frac{\partial \rho \bar{u}_i}{\partial t} + \frac{\partial}{\partial x_j}(\rho \bar{u}_i \bar{u}_j) = -\frac{\partial \bar{p}^*}{\partial x_i} + \frac{\partial}{\partial x_j}\left[(\mu + \mu_t)\left(\frac{\partial \bar{u}_i}{\partial x_j} + \frac{\partial \bar{u}_j}{\partial x_i}\right)\right] \tag{3}$$

In Eq. (3), the overbar denotes the filtered quantity, the asterisk denotes the modified pressure, Eq. (4), and μ_t is the turbulent viscosity. This term represents the energy dissipation present in the smallest scales of flow, which are not resolved in LES and must be modeled:

$$\mu_t = \rho(C\Delta^2)\bar{S} \tag{4}$$

Δ is the grid filter length and $\bar{S}$ is the filtered shear strain rate:

$$\bar{S} = \sqrt{\bar{S}_{ij}\bar{S}_{ij}}\ , \text{and } \bar{S}_{ij} = \frac{1}{2}\left(\frac{\partial \bar{u}_i}{\partial x_j} + \frac{\partial \bar{u}_j}{\partial x_i}\right) \tag{5}$$

$\bar{p}^*$ is the modified pressure:

$$\bar{p}^* = \bar{p} + \frac{2}{3}\rho\kappa \tag{6}$$

κ is the subgrid turbulence kinetic energy.

The numerical solution of the conservation equations (1) and (2) is accomplished by the computational code UNSCYFL3D (Unsteady Cyclone Flow 3D). This in-house tool is based on the finite volume method in unstructured three-dimensional grids, which enables the faithful representation of complex geometries. The SIMPLE (Semi-Implicit Method for Pressure-Linked Equations) algorithm is used to couple the velocity and pressure fields. In all the simulations carried out in this work the three-time-level scheme was used for time-advancement and the centered differencing scheme was employed for the advective and diffusive terms of the momentum equations. Aiming at a precise turbulence modeling, the dynamic Smagorinsky model was employed (Germano *et al*., 1990). In this model, the eddy viscosity coefficient is locally calculated to reflect closely the state of the flow. This is done by sampling the smallest resolved scales and using this information to model the sub-grid scales.

2.2 Discrete phase model

ISSN 2176-5480

The dispersed phase is treated in a Lagrangian framework, in which each particle is tracked through the domain and its equation of motion is based on Newton's second law. The trajectory and motion equations in the x-direction for a rigid, spherical particle can be written, respectively, as:

$$\frac{dx_p}{dt} = u_p \tag{7}$$

$$\frac{du_p}{dt} = F_D(u - u_p) + a \tag{8}$$

Similar equations can be written for the other two directions. In Eq. (8) the first term on the right hand side is the drag force experienced by the particle, F_D, given by Eq. (9), and a is the acceleration term, which contains only the gravitational and buoyancy forces – Eq. (10):

$$F_D = \frac{18\mu}{\rho_p d_p^2}\frac{C_D \,\mathrm{Re}_p}{24} \tag{9}$$

$$a = \frac{g(\rho_p - \rho)}{\rho_p} \tag{10}$$

Forces such as Saffman's, Basset and virtual force have been neglected. This is a reasonable assumption since the particle material density is nearly 1000 times the gas density (Crow, 2005; Brennen, 2005; Loth, 2009).

In Eq. (9), Re_p and C_D are the particle Reynolds number, given by Eq. (11), and the drag coefficient, respectively.

$$\mathrm{Re}_p \equiv \frac{\rho d_p \left|u_p - u\right|}{\mu} \tag{11}$$

The empirical correlations proposed by Schiller and Naumann, (1953) are used to evaluate the drag coefficient past each particle, which is assumed to be a smooth sphere:

$$C_D = \begin{cases} 24/\mathrm{Re}_p & for \quad \mathrm{Re}_p < 0.1 \\ 24(1 + 0.15\,\mathrm{Re}_p^{0.687})/\mathrm{Re}_p & for \quad 0.1 < \mathrm{Re}_p \le 1000 \\ 0.44 & for \quad \mathrm{Re}_p > 1000 \end{cases} \tag{12}$$

In the above equations, the subscript p denotes a discrete phase variable, and the continuous phase properties are interpolated to particle center of mass. In this work Sheppard's scheme was used.

If the drag force and fluid velocity are assumed constant during the particle time step, Eq. (8) can be integrated analytically. While this might sound as a brutal simplification, it is a reasonable approximation when the time step is small, which is typically used in LES and required when dealing with small Stokes numbers. The resulting equations for the particle velocity and position in the x-direction are then:

$$u_p^{n+1} = u^n + e^{-\Delta t/\tau_p}(u_p^n - u^n) - a\tau_p(e^{-\Delta t/\tau_p} - 1) \tag{13}$$

$$x_p^{n+1} = x^n + \Delta t(u^n + a\tau_p) + \tau_p(1 - e^{-\Delta t/\tau_p})(u_p^n - u^n - a\tau_p) \tag{14}$$

τ_p is the particle relaxation time, given by $1/F_D$. The superscript n+1 denotes the calculated variable at the new time step and the superscript n denotes the calculated variable at the previous time step. The particle relaxation time is associated with the time it takes for a particle to respond to a change in the flow. A massless particle, for instance, responds instantaneously to any change in the flow, and thus has the same local velocity as the fluid.

ISSN 2176-5480

Each particle is tracked by the particle-localization algorithm proposed by Haselbacher *et al*., 2007. This algorithm is based on tracking a particle along its trajectory by computing the intersections of the trajectory and the cell faces. Since it does not depend on the cell shape, it is very suitable for use in unstructured grids.

3. DEVELOPED STUDY

3.1 Cyclone geometry and grids

The dimensions of the cyclones are displayed in Fig. 1 and Tab. 1. These cyclones were investigated experimentally by R. Xiang et al., 2001.

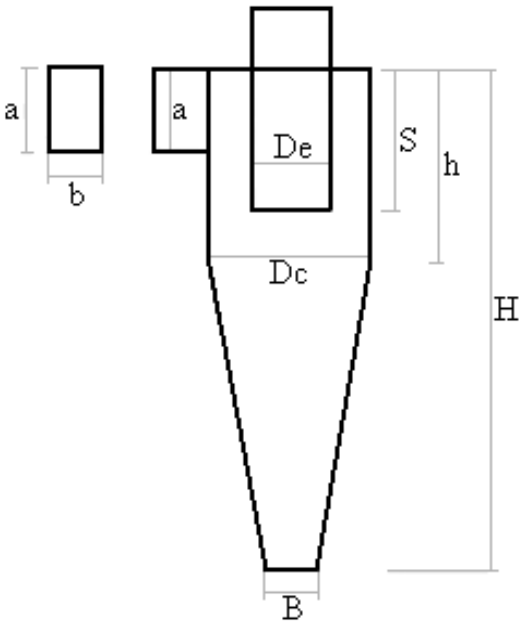

Figure 1. Cyclone geometry.

Table 1. Dimensions of the cyclones simulated.

Dimension	Cyclone 1 (m)	Cyclone 2 (m)
Body diameter, Dc	0.031	0.031
Gas outlet diameter, De	0.0155	0.0155
Inlet height, a	0.0125	0.0125
Inlet width, b	0.005	0.005
Cyclone height, H	0.077	0.077
Cylinder height, h	0.031	0.031
Gas outlet duct length, S	0.0155	0.0155
Cone bottom opening, B	0.0194	0.0116

The application of LES to any flow requires care, particularly regarding mesh quality and refinement, the order of numerical schemes and the time step size. Grid resolution must be high enough to compute the scales up to the inertial range of the energy spectrum. Two grids, with nearly 450,000 and 1,800,000 hexahedra, regarding only the cyclone body and a short overflow duct, were tested. Because no significant difference was found in both the average and RMS gas velocity profiles, this coarser mesh was used as a base mesh for the cyclone body. This way, although the total number of elements in the different grids - used to model the different tested geometries - ranged between 450,000 and 700,000 hexahedra, due to the different length and shape of the several simulated overflow duct configurations, the cyclone body meshing was held constant. This procedure was adopted to reduce the mesh influence on the results.

ISSN 2176-5480

For easy of understanding the main characteristics of all the performed simulations are displayed in Tab. 2. The definition of the overflow duct length, Ldo, of the position considered as the curve beginning, and curves radii are show in Fig 2.

Table 2. Description of all simulated cases.

Case Index	Nomenclature	Ldo [m]	Curve Angle [º]	Curve Radii [m]	Curve Beginning [m]
1	IntDuct_180_1	0,073	180	0,0155	0
2	IntDuct_180_2	0,073	180	0,02325	0
3	IntDuct_VSC1	0,073	90	0,0155	0
4	IntDuct_VSC2	0,073	90	0,02325	0
5	IntDuct_VSC3	0,073	90	0,03875	0
6	IntDuct_SC1	0,073	90	0,0155	0,013
7	IntDuct_SC2	0,073	90	0,02325	0,013
8	IntDuct_SC3	0,073	90	0,03875	0,013
9	LongDuct_180_1	0,1046	180	0,0155	0
10	LongDuct_180_2	0,1046	180	0,02325	0
11	LongDuct_VSC1	0,1046	90	0,0155	0
12	LongDuct_VSC2	0,1046	90	0,02325	0
13	LongDuct_VSC3	0,1046	90	0,03875	0
14	LongDuct_SC1	0,1046	90	0,0155	0,013
15	LongDuct_SC2	0,1046	90	0,02325	0,013
16	LongDuct_SC3	0,1046	90	0,03875	0,013
17	LongDuct_LC1	0,1046	90	0,0155	0,043
18	LongDuct_LC2	0,1046	90	0,02325	0,043
19	LongDuct_LC3	0,1046	90	0,03875	0,043
20	ShortDuct	0,043	0	#	#
21	IntDuct	0,073	0	#	#
22	LongDuct	0,1046	0	#	#
23	VeryLongDuct	0,1346	0	#	#
24	VeryLongDuct2	0,1646	0	#	#
25	VeryLongDuct3	0,1946	0	#	#
26	VeryLongDuct4	0,2246	0	#	#
27	ShortDuct_Cy1	0,043	0	#	#
28	IntDuct_Cy1	0,073	0	#	#
29	LongDuct_Cy1	0,1046	0	#	#
30	VeryLongDuct_Cy1	0,1346	0	#	#

In Tab. 2, cases with the termination "Cy1" - lines 27 to 30 - refer to cyclone 1, whose dimensions are describe in Tab. 1, column 2. All the other cases refer to cyclone 2, dimensions shown in Tab. 1, column 3. Terminations VSC, SC and LC refers to the overflow duct curve beginning position:

- ✓ VSC: The curve begins at the cyclone top plan;
- ✓ SC: The curve begins at 0.013 m from the cyclone top plan;
- ✓ LC: The curve begins at 0.043 m from the cyclone top plan.

The grade efficiency curve obtained in each simulation was compared with experimental results by R. Xiang *et al*., (2001). Unfortunately it was not possible to reproduce, exactly, the experimental conditions, once no additional information regarding the overflow duct were provided in the experimental work. Also, R. Xiang *et al*., (2001) did not measure the fluid velocity inside the cyclones in their work, however, as a part of the study carried out here, the mean and RMS velocity and pressure profiles were analyzed in the following axial stations:

- o Plane x = 0: in y = 0.03 m and y = 0.05 m;

ISSN 2176-5480

- Plane z = 0: in y = 0.03 m and in y = 0.05 m.

See Fig. 3 for more details.

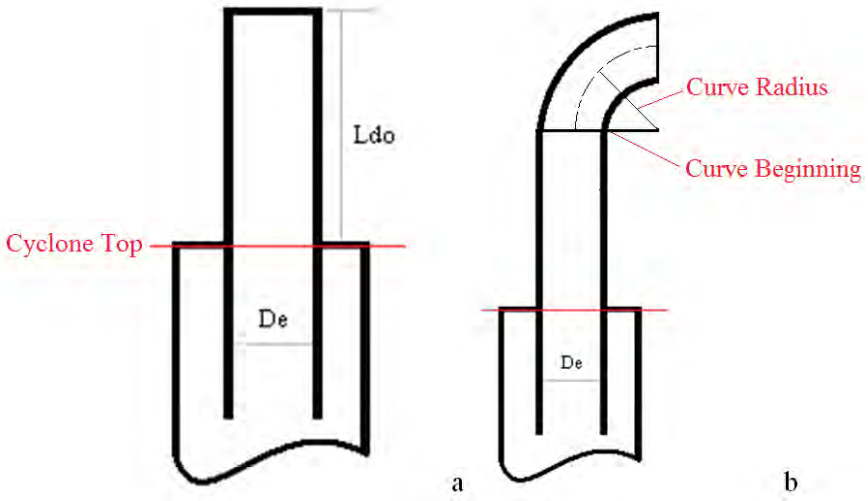

Figure 2. (a) Overflow duct length definition. (b) Curve beginning and curve radius definitions.

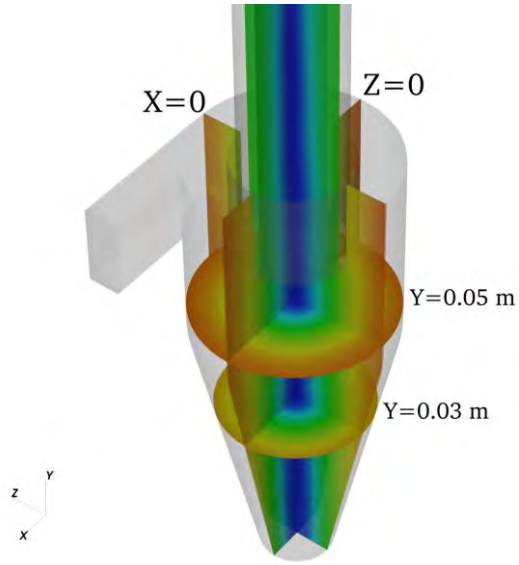

Figure 3. Plane position where the velocity and pressure profiles were analyzed.

The analyzed velocity and pressure profiles showed no clear tendency, actually, in most cases only small differences in the average profiles were observed. Regarding the RMS profiles, some cases presented considerably differences for the peak values (located at the cyclone center), but in general, only small differences were obtained outside the central region. Based on this information, these profiles are omitted in the present work.

An overview of the different outlet duct configurations may be seen in Fig. 4, where the grids used in cases 1 to 16 from Tab. 2 are shown and in Fig. 5 where the numerical grids used in simulations 20 to 30 from tab. 2 are shown.

3.2 Simulations steup

The fluid phase was treated as air with constant density 1.205 Kg/m³ and viscosity 1.82 x 10^{-5} Kg/m.s. A uniform velocity profile (U_{in}) was prescribed at the inlet. At the overflow outlet the static pressure was prescribed and all the cyclone walls were considered as no-slip boundaries. The simulated flow rate for each cyclone was: 40 l/min.

Monodisperse polystyrene latex particles with density 1,050 kg/m³ and diameters ranging from 0.5 to 6.0 μm were injected with the same velocity as the fluid in the cyclone inlet. For each diameter, a total of 11,132 particles were fed into the cyclone, which were uniformly distributed at the inlet boundary. At the solid surfaces, particles were reflected considering a perfectly elastic collision. An exception is made for the cyclone bottom wall. Particles touching this

ISSN 2176-5480

specific wall are considered collected. Particles that crossed the overflow face were considered escaped and deleted from the calculation. The particle Stokes number, given by Eq. (15), and the particle relaxation time are shown in Tab. 3 as functions of the particle diameter. A time step of 10 microseconds for the fluid phase and 0.25 microseconds for the particulate phase was employed.

$$St = (\rho_p - \rho)\frac{d_p^2 U_{in}}{18\mu D_c} \tag{15}$$

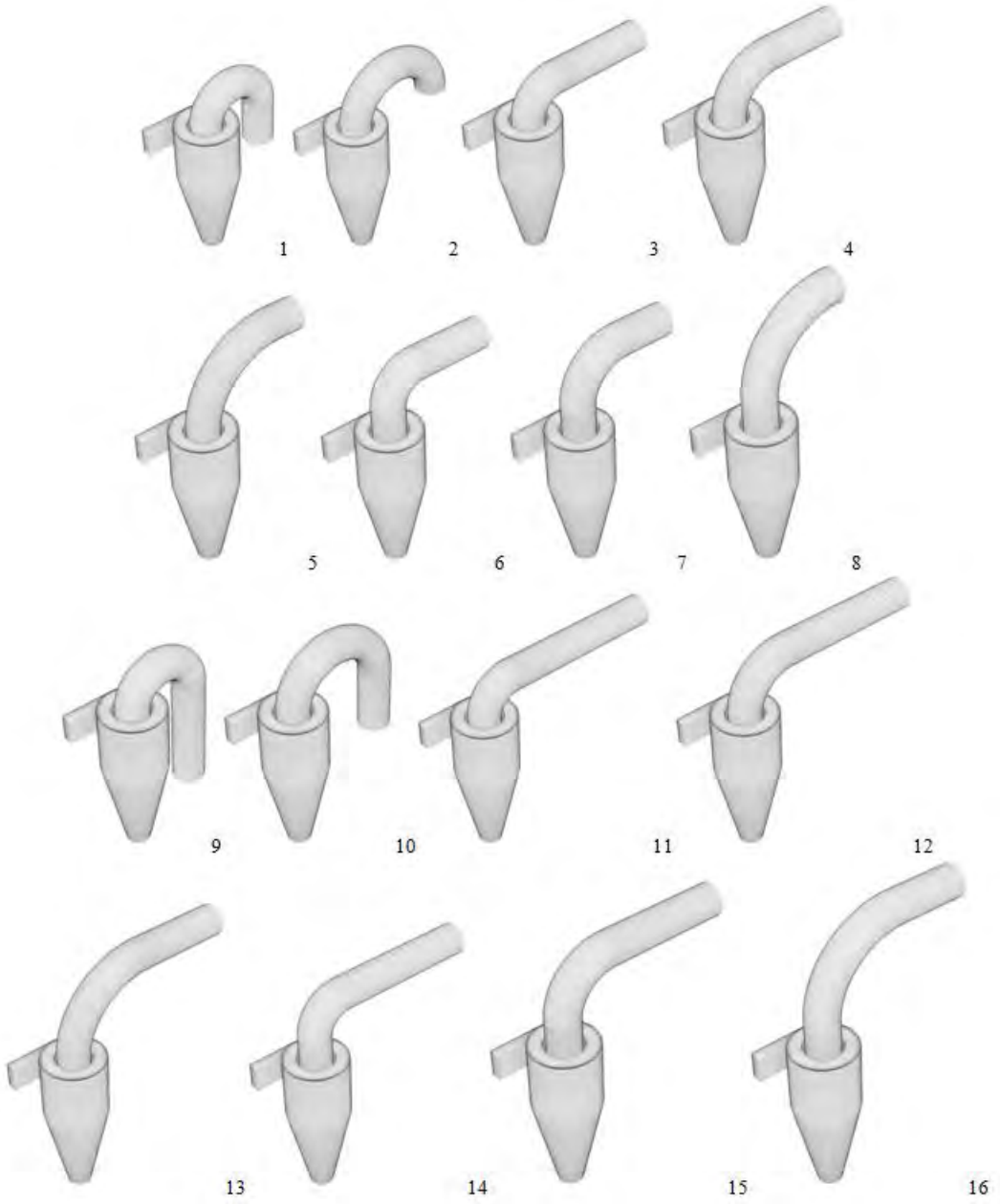

Figure 4. Grids used in cases 1 to 16 from Tab. 2.

ISSN 2176-5480

Table 3: Stokes number and relaxation time for the particle diameters investigated.

Particle diameter (μm)	Particle Stokes Number	Particle Relaxation Time (μs)
0.5	2.75×10^{-4}	0.801
1.0	1.10×10^{-3}	3.21
1.5	2.48×10^{-3}	7.21
2.0	3.66×10^{-3}	12.8
2.5	6.89×10^{-3}	20.0
3.0	9.92×10^{-3}	28.8
3.5	1.35×10^{-2}	39.3
4.0	1.76×10^{-2}	51.3
4.5	2.23×10^{-2}	64.9
5.0	2.75×10^{-2}	80.1
5.5	3.33×10^{-2}	97.0
6.0	3.97×10^{-2}	115

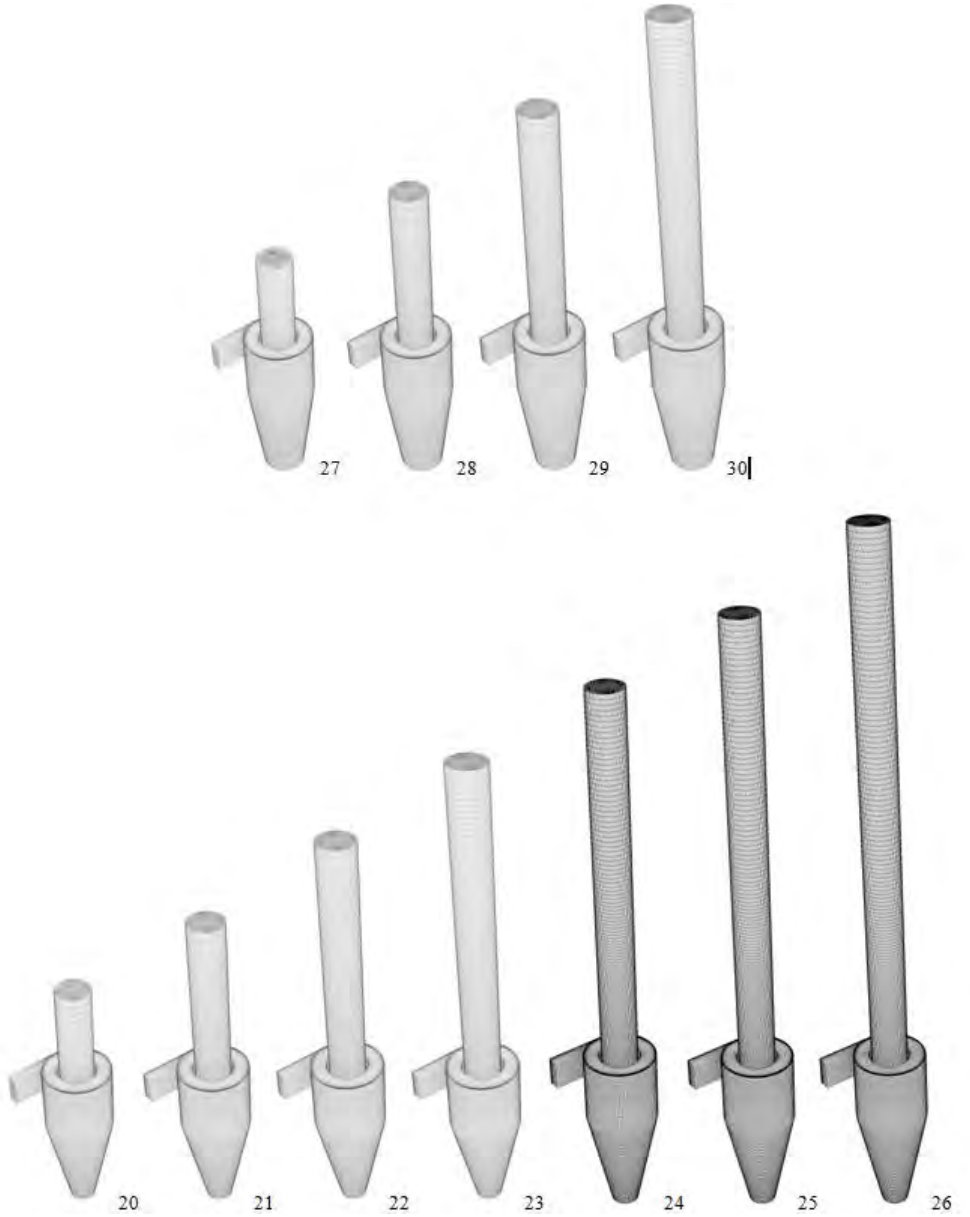

Figure 5. Grids used in cases 20 to 30 from Tab. 2.

ISSN 2176-5480

4. RESULTS

The obtained results for the pressure drop and cut off diameter for the different simulated cases are shown in Tab 3. The imposed pressure in the outlet plane is equal to zero, so the pressure drop in the cyclone was computed as the average pressure in the inlet. In this work the average pressure was computed at the plane X=0.016 m. The experimental values reported by R. Xiang et al., 2001 for the pressure drop and cut off diameter for cyclone 2, are, respectively, 196 Pa and 1,91 μm.

Table 3. Comparison between the numerical simulated cases and the experimental values for pressure drop and cut off diameter.

Case	Nomenclature	Pressure Drop [Pa]	Difference ΔP [%]	Cut Off Diameter [μm]	Difference C.O.D [%]
1	IntDuct_180_1	197,30	0,70	1,62	15,18
2	IntDuct_180_2	202,12	3,16	1,62	15,18
3	IntDuct_VSC1	194,14	-0,92	1,61	15,71
4	IntDuct_VSC2	203,75	3,99	1,61	15,71
5	IntDuct_VSC3	209,96	7,15	1,54	19,37
6	IntDuct_SC1	198,38	1,25	1,67	12,57
7	IntDuct_SC2	204,54	4,39	1,53	19,90
8	IntDuct_SC3	209,61	6,98	1,61	15,71
9	LongDuct_180_1	196,73	0,40	1,62	15,18
10	LongDuct_180_2	205,54	4,90	1,58	17,28
11	LongDuct_VSC1	193,37	-1,31	1,59	16,75
12	LongDuct_VSC2	203,20	3,71	1,54	19,37
13	LongDuct_VSC3	209,77	7,06	1,50	21,47
14	LongDuct_SC1	197,65	0,88	1,62	15,18
15	LongDuct_SC2	203,34	3,78	1,57	17,80
16	LongDuct_SC3	210,68	7,53	1,52	20,42
17	LongDuct_LC1	195,58	-0,18	1,54	19,37
18	LongDuct_LC2	201,83	3,01	1,59	16,75
19	LongDuct_LC3	208,12	6,22	1,53	19,90
20	ShortDuct	231,63	18,22	1,46	23,56
21	IntDuct	216,90	10,70	1,56	18,32
22	LongDuct	212,98	8,70	1,58	17,28
23	VeryLongDuct	212,09	8,25	1,52	20,42
24	VeryLongDuct2	211,81	8,10	1,49	21,99
25	VeryLongDuct3	212,59	8,50	1,59	16,75
26	VeryLongDuct4	213,25	8,84	1,64	14,14

The data shown in Tab. 3 indicate some interesting points, and therefore part of these are reproduced below in the form of graphs. The first analysis involves the pressure drop and the cut off diameter in the cyclone as a function of the outlet duct length, considering only straight ducts, cases 20 to 26 from Tab. 3. The data is disposed in Fig. 6.

Observing Fig. 6 (b) note that the pressure drop decreases as the length of the simulated duct increases, although this may seem counter-intuitive, it is in fact consistent with the expected, once in confined swirling flows, the main cause of the pressure drop isn't friction with the walls of the separator, but the fact that much of the static pressure, p, is transformed into dynamic pressure, $\frac{1}{2}\rho v^2$, due to the strong swirling motion (Hoffmann and Stein, 2008). Extending the outlet duct from a short to a long duct, the vortex "loses strength", in a way that part of the static pressure does not transform into dynamic pressure any more, this considerably reduces the pressure drop. Extending further the outlet duct, from a long to a very long duct, the tangential velocity profiles (not shown here) show that the generated vortex does not change considerably, this partially explains the small variation obtained for the average pressure profiles in this case. Extending even more the outlet duct, the pressure drop starts to increase, this may be seen as the effect of the gas friction with the walls overlapping the effect of dynamic pressure reduction. Should be noted that according to

ISSN 2176-5480

Hoffmann and Stein, 2008, the pressure recovery due to the reduction of the swirl movement along the pipe upstream the separator, due to the gas friction with the walls (or by mixture effects) is minimal.

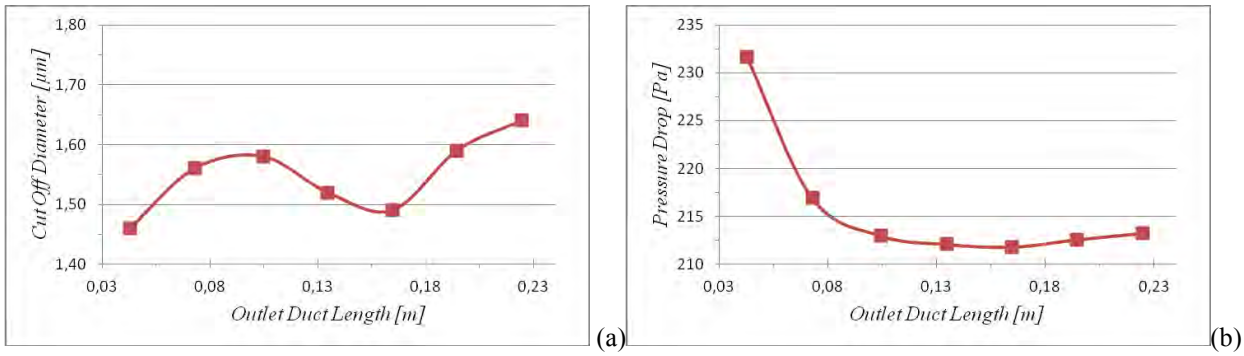

(a) (b)

Figure 6. Cut off diameter (a) and pressure drop (b) as function of the outlet duct length.

Considering now the cyclone cut off diameter. Fig. 6(a), we note that the obtained behavior is at least complex, and interpretation of such results should be done carefully. It is known that the first two points of the graph, which are related to the smaller outlet duct lengths, can be influenced by the subcritical regime in the output plane, and thus "contaminated" by purely numerical effects. With respect to the other three points, outlet duct with length: 0.1046, 0.1346 and 0.1646 m, these indicate that the cyclone efficiency increased with the outlet duct length. But for even longer outlet ducts, the cyclone efficiency decreased again. This behavior demonstrates the importance of the outlet duct length in the cyclone efficiency. Within the tested limits, a 36% variation in the outlet duct length (from case 24 to 26 -Table 2) resulted in a 10% variation in the cyclone cut off diameter.

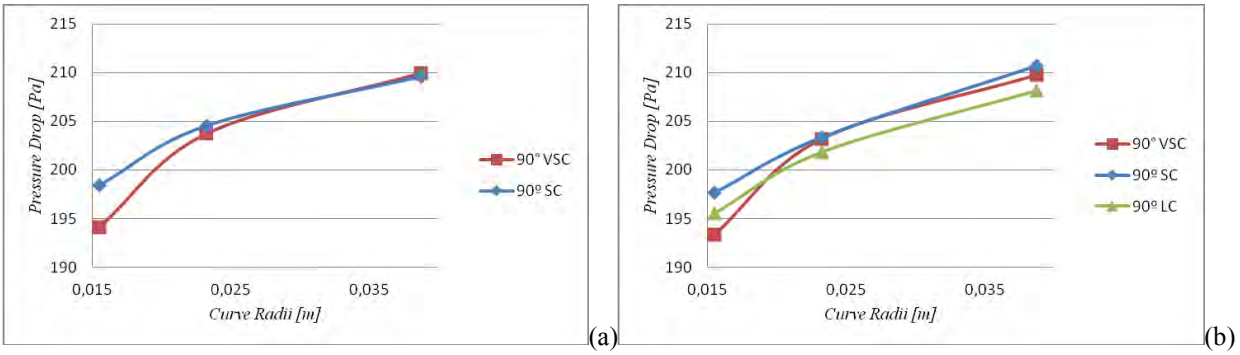

(a) (b)

Figure 7. Pressure drop as a function of curve radius. Cases 3-8(a) and 11-19(b) from tab. 2.

Figure 7 shows the pressure drop as a function of curve radius for cases 3-8 (a), and 11-19 (b), from Tab. 2. This figure enables the verification of the behavior of the pressure drop as function of the curvature radii and of the start position of such curves in the outlet duct. It can be easily seen that the obtained behavior is quite similar in all cases - the smaller the curvature radii, at least within the tested limits, the lower the pressure drop. This is because the curve tends to decrease the intensity of the swirl motion, and, consequently, reduces the dynamic pressure, Fig. 9.

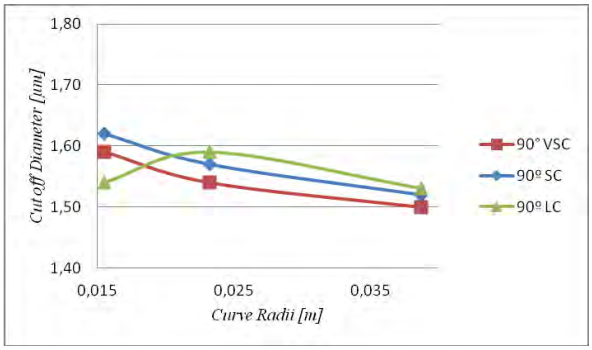

Figure 8. Cut off diameter as a function of curve radius. Cases 11-19(b) from tab. 2.

ISSN 2176-5480

Figure 8 presents the cut off diameter as a function of curve radii. Note that, generally, the cyclone efficiency decreases as the curve radii from the outlet duct decreases. this behavior agrees with the one presented in Fig. 7(b), for the pressure drop: A smaller radii leads to a lower pressure drop and also a lower collection efficiency.

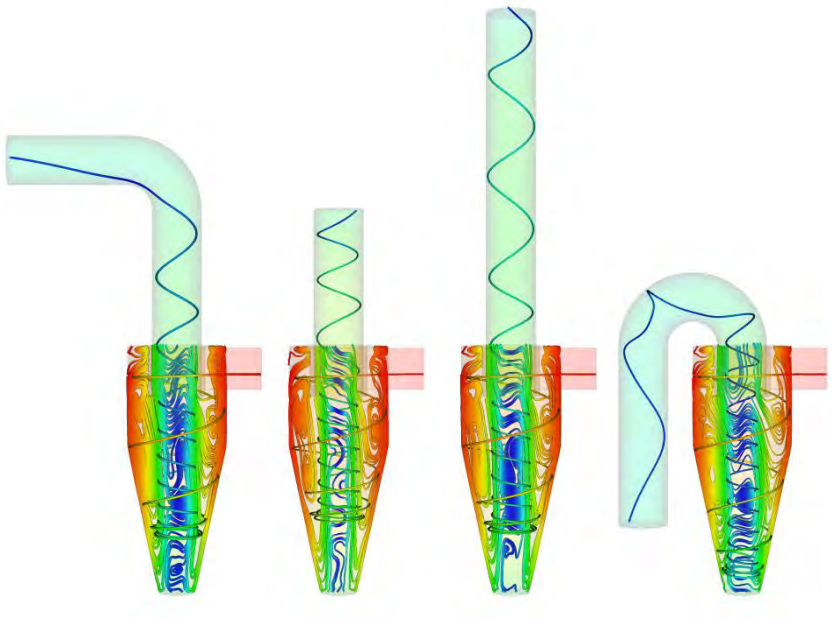

Figure 9. Effect of the outlet duct length and shape on the stream lines.

5. CONCLUSIONS

A study on the effects of the outlet duct flow inside the cyclone was performed. This study included thirty simulations, where different outlet duct configurations were used. All the simulations performed in this work are based on the LES methodology, with the dynamic sub-grid turbulence model. The dispersed phase, treated in a Lagrangiam reference frame, was simulated in a concomitant manner. Although expensive from a computational point of view, the methodology adopted allowed the gas-solid simulations to be independent of any ad-hoc parameters. The mesh in the separator body was held constant throughout the work, ensuring minimal influence from one simulation to another. The results shown that the outlet duct length and shape do influence the cyclone flow field, as previous stated by Schmidt *et al*., 2004. It was also demonstrated that even small modifications in the outlet duct may produce considerable differences in the cyclone efficiency. The pressure drop behavior, when combined with the swirl motion intensity, matched the behavior describe by Hoffmann and Stein, 2008. But the cut off diameter showed a complicated relation, emphasizing the necessity of continuity of the present study.

6. ACKNOWLEDGEMENTS

The authors would like to thank: FAPEMIG, CAPES and PETROBRAS for the financial support.

7. REFERENCES

Azadi, M., Azadi, M., Mohebbi, A., 2010. "A CFD study of the effect of cyclone size on its performance parameters", *Journal of Hazardous Materials*, vol. 182, p. 835-841.

Bernardo, S., “Estudo dos escoamentos gasoso e gás-sólido em ciclones pela aplicação de fluidodinâmica computacional”, 2005, 240 f., Tese de Doutorado, Universidade Estadual de Campinas, São Paulo, Brasil.

Bernardo, S., Mori, M., Peres, A. P., Dinisio, R. P., 2006." 3-D computational fluid dynamics for gas and gas-particle flows in a cyclone with different inlet section angles", *Power Tech.*, vol. 162, p. 190-200.

Bhaskar, K.U., Y.R. Murthy, N. Ramakrishnan, J.K. Srivastava, S. Sarkar and V. Kumar, 2007. "CFD validation for flyash particle classification in hydrocyclones", *Miner. Eng.*,vol. 20, p. 290-302.

Brennen, E. C., “Fundamentals of multiphase flow” Cambridge University Press, 2005.

Chuah, T.G., Gimbun, J. and Choong, T.S.Y., 2006, “A CFD study of the effect of cone dimensions on sampling aerocyclones performance and hydrodynamics”, *Power Technology*, Vol. 162, pp. 126-132.

Crowe, T. C. “Multiphase flow handbook”, CRC, 2006

ISSN 2176-5480

Derksen, J.J., 2003, “Separation performance predictions of a Stairmand high-efficiency cyclone”, *Fluid Mechanics and Transport Phenomena*, Vol. 49, no 6, pp. 1359-1371.

Derksen, J.J., Sundaresan, S. and van den Akker, H.E.A., 2006, “Simulation of mass-loading effects in gas-solid cyclone separators”, *Power Technology*, Vol. 163, pp. 59-68.

Derksen, J.J., van den Akker, H.E.A., Sundaresan, S., 2008, " Two-way coupled Large-Eddy simulations of the gas-solid flow in cyclone separators", *American Institute of Chemical Engineers*, vol. 54, p. 872-884.

Dias, D. B., Mori, M., Martigninoni, W. P., 2009, "Boundary conditions effects in CFD cyclone simulations", *WCC8.*

Elsayed, K., Lacor, C., 2013a, "CFD Modeling and Multi-Objective Optimization of Cyclone Geometry Using Desirability Function, Artificial Neural Networks and Genetic Algorithms", *Applied Mathematical Modelling*, vol. 37, p. 5680-5704.

Elsayed, K., Lacor, C., 2013b, "The Effect of Cyclone Vortex Finder Dimensions on the Flow Pattern and Performance using LES", *Computer & Fluids*, vol. 71, p. 224-239.

Germano, M., Piomelli, U., Moin, P., Cabot, W. H., 1990, "A dynamic subgrid-scale eddy viscosity model", *American Institute of Physics*., vol. 7, p. 1760-1795.

Haselbacher, A., Najjar, F.M. and Ferry, J.P., 2007, “An efficient and robust particle-localization algorithm for unstructured grids”, *Journal of Computational Physics*, Vol. 225, pp. 2198-2213.

Hoekstra, A.J., Derksen, J.J. and Van den Akker, H.E.A.,1999, “An experimental study of turbulent swirling flow in gas cyclones”, *Chemical Engineering Science*, Vol. 54, pp. 2055-2065.

Hoffman, A.C., Stein, L.E., 2008, “Gas cyclones and swirl tubes – principles, design and operation”, Second Edition, Springer – Verlag Berlin Heidelberg.

J. Jiao, Y. Zheng, G. Sun, J. Wang, 2006, "Study of the separation efficiency and the flow field of a dynamic cyclone", *Separation and Purification Technology*, vol. 49, p. 157-166.

Kepa, A., 2010, "Divison of outlet flow in a cyclone vortex finder – the CFD calculations", *Separation and Purification Technology*., vol. 75, p. 127-131.

Loth, E., Computational fluid dynamics of bubbles, drops and particles, Cambridge University Press, 2009

Martignoni, W. P., Bernardo, S. and Quintani, C. L., 2007, “Evaluation of cyclone geometry and its influence on performance parameters by computational fluid dynamics (CFD)”, *Brazilian journal of chemical engineering*, v. 24, p. 83-94.

Noriler, D., Vegini, A. A., Soares, C., Barros, A. A. C., Meier, H. F. and Mori, M., 2004, “A new role for reduction in pressure drop in cyclones using computational fluid dynamics techniques”, *Brazilian Journal of Chemical Engineering*, v.21, p. 93-101.

Raoufi, A., Shams, M., Farzaneh, M. , Ebrahimi, R., 2008, "Numerical simulation and optimization of fluid flow in a cyclone vortex finder", *Chemical Engineering and Processing*, vol. 47, p. 128-137.

Shi, L and Bayless, 2007, "Comparison of boundary conditions for predicting the collection efficiency of cyclones", *Powder Technology,* vol. 173, p. 29-37.

Schiller, L. and Naumann, Z., 1935, Ver. Deutsh. Ing. 77, 318.

S. Schmidt, H. M. Blackburn, M Rudman, 2004, "Impact of outlet boundary conditions on the flow properties within a cyclone", *15th Australasian Fluid Mechanics Conference*, December 13-17, Sydney, Australia.

S. Schuetz, G. Mayer, M. Bierdel, M. Piesche, 2004, "Investigations on the flow and separation behavior of hydrocyclones using computational fluid dynamics", *Int. J. Miner. Process.*, vol. 73, p. 229-237.

Xiang, R., Park, S.H. and Lee, K.W., 2001, “Effects of cone dimension on cyclone performance”, Journal of Aerosol Science, Vol. 32, pp. 549-561.

Yoshida, H., Nishimura, Y., Fukui, K., Yamamoto T., 2010, "Effect of apex cone shape on fine particle classification of gas-cyclone", *Powder Technology*, vol. 204, p. 54-62.

Zhao, B., Su, Y. and Zhang, J., 2006, “Simulation of gas flow pattern and separation efficiency in cyclone with conventional single and spiral Double inlet configuration”, *Chemical Engineering Research and Design*, v. 84(A12), p. 1158-1165.

8. RESPONSIBILITY NOTICE

The author are the only responsible for the printed material included in this paper.